Journal of Photochemistry and Photobiology A: Chemistry 231 (2012) 33–40

Contents lists available at SciVerse ScienceDirect

Journal of Photochemistry and Photobiology A: Chemistry

journal homepage: www.elsevier.com/locate/jphotochem

Photochemistry of $CF_3(CH_2)_2CHO$ in air: UV absorption cross sections between 230 and 340 nm and photolysis quantum yields at 308 nm

M. Antiñolo, E. Jiménez, J. Albaladejo*

Universidad de Castilla-La Mancha, Departamento de Química Física, Facultad de Ciencias Químicas, Avda. Camilo José Cela, s/n, 13071 Ciudad Real, Spain

ARTICLE INFO

Article history:
Received 22 July 2011
Received in revised form
13 December 2011
Accepted 21 December 2011
Available online 10 January 2012

Keywords:
Atmospheric photodegradation
Fluorinated aldehyde
Absorption cross sections
Quantum yields
Photoproducts

ABSTRACT

This work constitutes the first study on the photochemical degradation process of $CF_3(CH_2)_2CHO$. Firstly, the wavelength and temperature dependence of the UV absorption cross sections, σ_λ, was determined. The $n \rightarrow \pi^*$ electronic transition band of C=O chromophore was characterized between 230 and 340 nm in the 269–323 K range. A hyperchromic effect was observed in the structured part of the band when the temperature decreases. Maximum $\sigma_{\lambda=283,\,291\,nm}$ at 323 K is ca. 22% larger than those at 269 K. Secondly, the pulsed laser photolysis of a stationary mixture of $CF_3(CH_2)_2CHO$/cyclohexane (OH-scavenger)/air or N_2 was carried out at 308 nm. On-line Fourier transform infrared (FTIR) spectroscopy was employed to monitor the decay of $CF_3(CH_2)_2CHO$ and to obtain the photolysis quantum yield, $\Phi_{\lambda=308\,nm}$, as a function of total pressure (20.5–760 Torr). A slight curvature in the Stern–Volmer plot was observed at pressures lower than 75 Torr. At high pressures, the pressure dependence of $\Phi_{\lambda=308\,nm}$ can be described by a Stern–Volmer relationship. Photodissociation of $CF_3(CH_2)_2CHO$ at 308 nm can produce HCO and $CF_3(CH_2)_2$ radicals (1a), $CF_3CH_2CH_3$ and CO (1b) and $CF_3(CH_2)_2CO$ radicals and H atoms (1c). HCO radicals are rapidly converted into CO in the presence of O_2. Formation of CF_3CH_2CHO and $CF_3CH_2CH_2OH$ evidences the importance of secondary chemistry involving $CF_3(CH_2)_2$ radicals formed in channel (1a). Further photodegradation of CF_3CH_2CHO yields mainly CF_3CHO. Small quantities of HC(O)OH were also detected. $CF_3(CH_2)_2C(O)OH$ was only observed in the absence of OH-scavenger, implying that formation of $CF_3(CH_2)_2CO$ radicals in channel (1c) is not an important photolysis pathway. Consequently, photodissociation of $CF_3(CH_2)_2CHO$ in the actinic region is a source of shorter fluorinated oxygenated compounds, but it is not expected to be a source of fluorinated acids.

1. Introduction

High global warming potential (GWP) gases are emitted from a variety of industrial processes including aluminum production, semiconductor manufacturing, electric power transmission, etc. [1]. In addition, some high GWP gases, such as hydrofluorocarbons (HFCs) are expected to replace a significant portion of past and current demand for chlorofluorocarbons (CFCs) and hydrochlorofluorocarbons (HCFCs) in many applications. Together with the global effect of the HFC emissions on the Earth's warming, the atmospheric degradation of these species yields trifluoroacetyl fluoride ($CF_3C(O)F$, TFF), which is hydrolyzed producing trifluoroacetic acid ($CF_3C(O)OH$, TFA) [2,3]. High concentrations of TFA have been observed in contemporary water and air samples, suggesting the existence of one or more large unknown sources. Partially fluorinated aldehydes, $CF_3(CH_2)_{x\geq0}CHO$, can be formed in the atmosphere from the reaction of potential HFC replacements, $CF_3(CH_2)_{x\geq0}CH_2OH$, with hydroxyl (OH) radicals and Cl atoms [4–7]. An additional source of TFA could be the further oxidation and/or photodegradation of $CF_3(CH_2)_{x\geq0}CHO$. For CF_3CHO and CF_3CH_2CHO, both the kinetics of the OH-initiated reactions [8–11] and the UV photolysis [11–14] have been previously studied. In contrast, only the OH-initiated oxidation for $CF_3(CH_2)_2CHO$ has been recently reported by our group, but no photochemical information is available in the actinic region ($\lambda \geq 290$ nm) [10]. Although no product studies for the OH + $CF_3(CH_2)_2CHO$ reaction are reported up to date, it is expected that CF_3CH_2CHO is the main product under low-NO_x conditions (similar to CF_3CHO and CF_3CH_2CHO) [5–7]. To assess the contribution of the photolytic loss of $CF_3(CH_2)_2CHO$ to the formation of smaller aldehydes or other species, such as fluorinated carboxylic acids (FCAs), it is important to measure the photolysis rate and the end-products under tropospheric conditions of temperature and pressure.

In this work, firstly, ultraviolet absorption cross sections (σ_λ) of $CF_3(CH_2)_2CHO$ were measured between 230 and 340 nm as a function of temperature (T = 269–323 K) in order to quantify the absorption process. The measured absorption cross section for $CF_3(CH_2)_2CHO$ at 308 nm was used to derive the photolysis quantum yields ($\Phi_{\lambda=308\,nm}$) as a function of pressure (20.5–760 Torr) in the presence of synthetic air or N_2. UV

* Corresponding author. Tel.: +34 926 29 53 27; fax: +34 926 29 53 18.
E-mail address: Jose.Albaladejo@uclm.es (J. Albaladejo).

1010-6030/$ – see front matter © 2012 Elsevier B.V. All rights reserved.
doi:10.1016/j.jphotochem.2011.12.023

photolysis of this hydrofluoroaldehyde can proceed by these three channels:

$$CF_3(CH_2)_2CHO + h\nu(\lambda = 308\,nm) \rightarrow CF_3(CH_2)_2 + HCO \quad (1a)$$

$$\rightarrow CF_3CH_2CH_3 + CO \quad (1b)$$

$$\rightarrow CF_3(CH_2)_2CO + H \quad (1c)$$

End-products formed from the secondary chemistry involving radicals formed in reaction (1) were also identified and quantified to evaluate the importance of each photolysis channel and the atmospheric implications of this degradation route.

2. Experimental details

The experimental set-ups employed in this study have been described in detail previously [14–17]. The experimental system based on the UV absorption spectroscopy has been previously employed for determining the absorption cross sections of different carbonyl compounds [15–17]. On the other hand, the experimental system for determining photolysis quantum yields has been used in our recent study on the photolysis of CF_3CH_2CHO [14]. Therefore, only a brief description of both set-ups is given below.

2.1. Ultraviolet (UV) absorption spectroscopy of $CF_3(CH_2)_2CHO$

The Beer–Lambert's law was used to determine the absorption cross sections σ_λ at different wavelengths λ (in base e):

$$A_\lambda = -\ln\left(\frac{I}{I_0}\right)_\lambda = \sigma_\lambda \ell c \quad (E1)$$

Transmitted intensities (I) from a deuterium lamp (continuous radiation in the 200–800 nm range) were first recorded in the absence of absorber (I_0). This radiation was dispersed by a 300 grooves/mm grating of a 0.5-m spectrograph with an instrumental resolution of 0.17 nm. The dispersed radiation was detected by a couple-charged device. The wavelength calibration was performed by means of a low-pressure Hg lamp (see Fig. 1a). After filling a jacketed Pyrex absorption cell (path length, ℓ = 107 cm) with a known concentration of $CF_3(CH_2)_2CHO$ (pressure in the cell ranged from 1.0 to 9.7 Torr), the transmitted intensity (I) of the white radiation from the D_2 lamp was recorded between 200 and 400 nm [14–17]. Absorbances (in base e), A_λ, were then calculated to obtain the absorption spectra at each pressure, p, and temperature, T (269–323 K). The temperature regulation was provided by a fluid circulating by means of a thermostatic bath (Huber, Polystat CC1) was used through the outer jacket (water was used at $T \geq 298$ K and ethanol at $T < 298$ K). Some examples of the absorption spectra at 273 K are presented in Fig. 1a. The absorption cross sections at each wavelength between 230 and 340 nm were obtained from the slope of A_λ versus p plots, according to Eq. (E1). In Fig. 1b, several examples are depicted at three wavelengths (254 nm, maximum emission wavelength of the Hg lamp; 283 nm, one of the absorption peaks of $CF_3(CH_2)_2CHO$; and 308 nm, photolysis wavelength).

2.2. Pulsed laser photolysis of $CF_3(CH_2)_2CHO$

Diluted samples of $CF_3(CH_2)_2CHO$ were photolysed in static conditions by the pulsed 308-nm radiation from a XeCl excimer laser at a repetition rate, υ_{rep} = 10 Hz. The energy per pulse and cm^2, E_λ, was varied from 6.5 to 10.9 mJ $pulse^{-1}$ cm^{-2}. The employed photolysis cell (L = 10 cm; V = 31 mL) was recently described in our photochemical study on CF_3CH_2CHO [14]. The 10-cm photolysis cell was filled with a certain total pressure, p_T, of a fresh gas mixture consisting of $CF_3(CH_2)_2CHO$, cyclohexane, and synthetic air (75–760 Torr) or N_2 bath gas (20.5–170 Torr). Initial concentrations of aldehyde, $[CF_3(CH_2)_2CHO]_0$, ranged from 4.7×10^{15} to 8.9×10^{16} molecule cm^{-3}. All experiments in the presence of O_2 were performed with added cyclohexane ($[cyclohexane]/[CF_3(CH_2)_2CHO]_0$ = 24–35) to the hydrofluorinated aldehyde/air mixture to avoid any unwanted secondary chemistry by OH radicals. Typically, $[O_2]/[CF_3(CH_2)_2CHO]_0$ ratio ranged from 104 to 122.

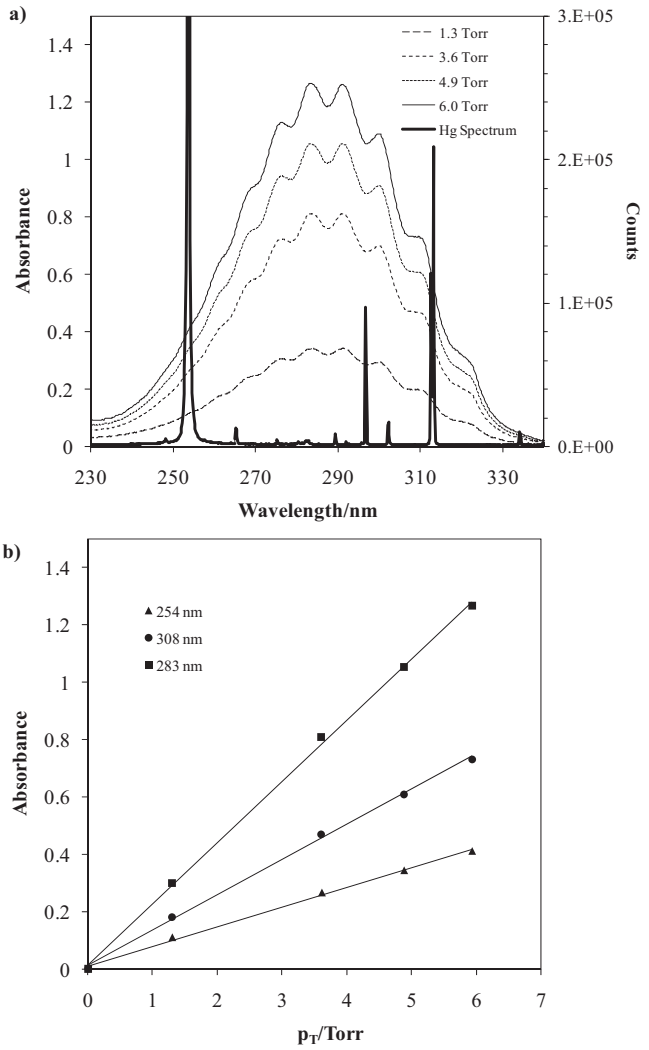

Fig. 1. (a) UV spectra $CF_3(CH_2)_2CHO$ recorded at 273 K as a function of pressure. The Hg lamp spectrum used in the wavelength calibration is overlapped. (b) Beer–Lambert plots at several wavelengths at 273 K.

The photolysis cell was completely irradiated and its inner wall was coated by a halocarbon wax to prevent any deactivation of the excited $CF_3(CH_2)_2CHO$ on the walls. Experiments performed with the uncoated cell yielded the same results, so thermal deactivation on the walls is not an important process.

After the photolysis of $CF_3(CH_2)_2CHO$, the content of the photolysis cell was expanded to a multipass cell (V = 1.33 L and optical path length ℓ = 800 cm) to monitor the decay of $CF_3(CH_2)_2CHO$ and identify the end products formed by Fourier transform infrared (FTIR) spectroscopy [10,14,18]. As a consequence of the gas expansion in the 1.33-L IR cell, the total pressure (and, therefore, the aldehyde concentration) was largely reduced, what did not make possible to accurately measure the quantum yields at total pressures below 75 Torr with this IR cell. For that reason, a smaller single path IR cell (L = 10 cm, V = 100 mL) was used to measure the photolysis quantum yield at low pressures. In this system, the pressure reduction in the IR cell after the gas expansion is approximately 50% and initial aldehyde concentrations were higher.

Before and after the photolysis process, the FTIR spectrum of the gas mixture was recorded between 500 and 4000 cm^{-1} at a spectral resolution of 1 cm^{-1} using a liquid nitrogen cooled mercury cadmium telluride (MCT) detector. The fraction of $CF_3(CH_2)_2CHO$ photolyzed per pulse is given by $\Phi_\lambda \sigma_\lambda F_\lambda$, where Φ_λ is the photolysis quantum yield, σ_λ is the absorption cross section of the compound (cm^2 $molecule^{-1}$), and F_λ (in photons cm^{-2} $pulse^{-1}$). After one laser pulse, the fraction of $CF_3(CH_2)_2CHO$ remaining is:

$$\frac{[CF_3(CH_2)_2CHO]_1}{[CF_3(CH_2)_2CHO]_0} = 1 - \Phi_\lambda \sigma_\lambda F_\lambda \quad \text{(E2)}$$

where $[CF_3(CH_2)_2CHO]_1$ is the concentration after one pulse and $[CF_3(CH_2)_2CHO]_0$ is the initial concentration. For n photolysis pulses:

$$\frac{[CF_3(CH_2)_2CHO]_n}{[CF_3(CH_2)_2CHO]_0} = (1 - \Phi_\lambda \sigma_\lambda F_\lambda)^n \quad \text{(E3)}$$

The linearized form of the former equation can be written as:

$$\ln\left(\frac{[CF_3(CH_2)_2CHO]_0}{[CF_3(CH_2)_2CHO]_n}\right) = -n \ \ln(1 - \Phi_\lambda \sigma_\lambda F_\lambda) \quad \text{(E4)}$$

For small fractional photolysis (below 10^{-4} molecule/pulse), Eq. (E4) can be approximated by:

$$\ln\left(\frac{[CF_3(CH_2)_2CHO]_0}{[CF_3(CH_2)_2CHO]_n}\right) = \Phi_\lambda \sigma_\lambda F_\lambda n \quad \text{(E5)}$$

The initial concentration of $CF_3(CH_2)_2CHO$ is proportional to the integrated band intensity obtained in the dark (A_0) and after photolyzing the sample by n laser pulses, $[CF_3(CH_2)_2CHO]_n$ is proportional to A_n:

$$\ln\left(\frac{A_0}{A_n}\right) = \Phi_\lambda \sigma_\lambda F_\lambda n \quad \text{(E6)}$$

where F_λ is directly related with the laser fluence, E_λ ($mJ\,cm^{-2}$ $pulse^{-1}$). The selected band used to monitor the temporal evolution of $CF_3(CH_2)_2CHO$ was the C=O stretching band (1757–1723 cm^{-1}). Before the spectral analysis, the identified carbonyl photolysis products, CF_3CH_2CHO, CF_3CHO, and HC(O)OH, were subtracted from the raw spectrum.

At a certain total pressure, E_λ and, therefore, F_λ has to be accurately known in order to determine $\Phi_{\lambda=308\,nm}$. In this work, acetaldehyde (CH_3CHO) was used in back-to-back experiments (E_λ is constant) as a chemical actinometer. The decay of the CH_3CHO was monitored by measuring the integrated area of the IR absorption band between 1752 and 1710 cm^{-1}. For a given E_λ, the photolysis quantum yield of $CF_3(CH_2)_2CHO$ at 308 nm can then be obtained from the following equation:

$$\Phi_{CF_3(CH_2)_2CHO} = \Phi_{CH_3CHO} \frac{J(CF_3(CH_2)_2CHO) \times \sigma_{CH_3CHO}}{J(CH_3CHO) \times \sigma_{CF_3(CH_2)_2CHO}} \quad \text{(E7)}$$

where J is defined as:

$$J(s^{-1}) = \Phi_\lambda \sigma_\lambda F_\lambda \frac{n}{\nu_{rep}} \quad \text{(E8)}$$

The photolysis quantum yield of CH_3CHO at 308 nm and 1 bar was taken from Moortgat et al. ($\Phi_{CH_3CHO} = 0.36$) and the absorption cross section of the actinometer was taken as 3.3×10^{-20} cm^2 [19,20]. A difference of 20% was observed between the measured laser energy with a calorimetric disc and that obtained from the decay of CH_3CHO.

Reagents. Gases from Praxair were used as supplied: synthetic air (99.999%) and CO (99.998%). Liquid samples were used after degasification at 77 K (purities are given in brackets): $CF_3(CH_2)_2CHO$ (>97%), CF_3CH_2CHO (>97%) and $CF_3CH_2CH_2OH$ (>97%) from Apollo Scientific Ltd, cyclohexane (>99.9%) and CH_3CHO (99.5%), from Aldrich, and HC(O)OH (98–100%) from Riedel-de Häen. Solid $CF_3(CH_2)_2C(O)OH$ (>97% Fluorochem Ltd.) was introduced in the FTIR cell by flowing He through the powder contained in a glass flask to record a reference spectrum.

3. Results and discussion

This section has been divided into three subsections. The first one reports the wavelength and temperature dependence of the absorption cross sections of $CF_3(CH_2)_2CHO$. Since some of the detected products may interfere in the analysis of $CF_3(CH_2)_2CHO$ by Fourier Transform Infrared (FTIR) spectroscopy, the second subsection present a discussion of the results on the identification and quantification of the end-products. Finally, the pressure dependence of the photolysis quantum yields is discussed in Section 3.3. Stated uncertainties are only $\pm 2\sigma$ statistical.

3.1. Wavelength and temperature dependence of UV absorption cross sections of $CF_3(CH_2)_2CHO$

The average absorption cross sections between 230 and 340 nm are listed every nm as a function of temperature (269–323 K) in Table S1 of the supporting information. In Fig. 2a the weak and

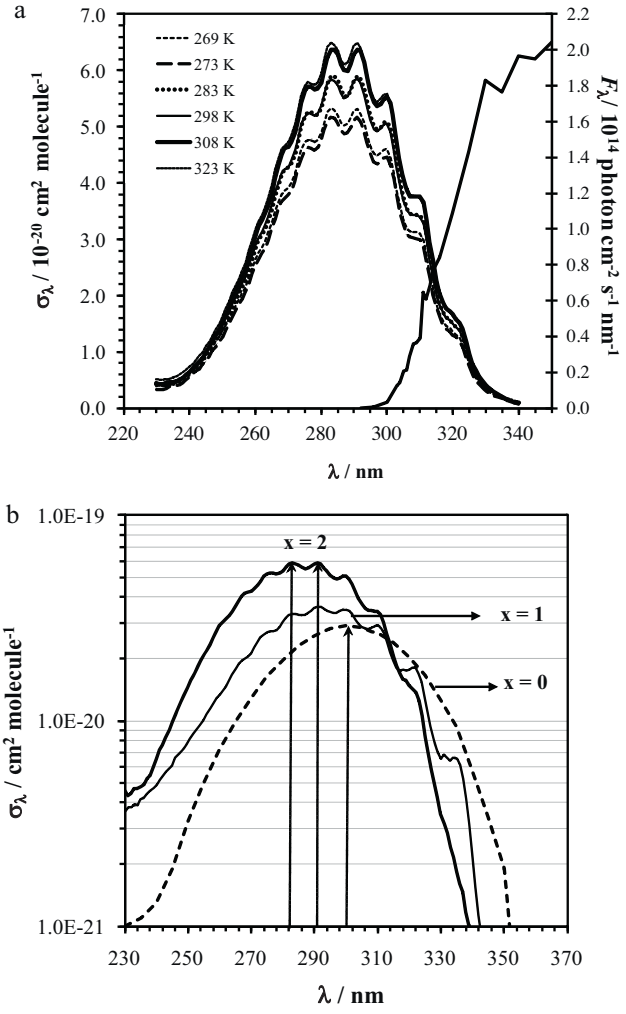

Fig. 2. (a) Wavelength (230–340 nm) and temperature (269–323 K) dependence of the absorption cross sections, σ_λ, for $CF_3(CH_2)_2CHO$. (b) Comparison among the UV absorption spectrum of $CF_3(CH_2)_xCHO$ at 298 K for $x = 0$ (dashed curve, Chiappero et al. [13]), $x = 1$ (solid curve, Antiñolo et al. [14]) and $x = 2$ obtained in this work. The dashed lines point to the maximum absorption cross sections.

Table 1
Maximum absorption cross sections for $CF_3(CH_2)_{x=0-2}CHO$ at 298 K.

Fluoroaldehyde	λ_{max}/nm	$\sigma_{\lambda max}/10^{-20}$ cm^2	Reference
$CF_3(CH_2)_2CH_3$	283.3 ± 0.9	5.84 ± 0.16	This work
	290.8 ± 0.8	5.85 ± 0.14	
CF_3CH_2CHO	290.82 ± 0.22	3.59 ± 0.24	Antiñolo et al. [14]
	293	3.64	Chiappero et al. [13]
	292	3.85	Sellevåg et al. [11]
CF_3CHO	300	2.89	Chiappero et al. [13]
	300	3.01	Hashikawa et al. [12]
	301	3.20	Sellevåg et al. [11]

structured absorption band corresponding to the $n \rightarrow \pi^*$ transition of the C=O group is shown at all studied temperatures. As it can be seen, a clear positive temperature dependence of σ_λ was observed, especially between 260 and 310 nm. Therefore, σ_λ increases with temperature. As can be seen in Fig. 2a, two maximum absorption peaks with equal absorption cross sections are located around 283 and 291 nm. $\sigma_{\lambda,max}$ at these wavelengths was found to range from 5.33×10^{-20} cm^2 molecule^{-1} at 269 K to 6.50×10^{-20} cm^2 molecule^{-1} at 323 K. The observed T-dependence of $\sigma_{\lambda,max}$ can be parameterized as follows:

$$\ln\ \sigma_\lambda(T) = 4.5 \times 10^{-3}\,(T - 298\,\mathrm{K}) + \ln\,\sigma_{\lambda,\max}\,(T = 298\,\mathrm{K}) \qquad \text{(E9)}$$

This absorption peak is conveniently coincident with 308 nm. For that reason, the quantum yield measurements were determined at that wavelength.

Fig. 2b shows a comparison among the absorption spectra for $CF_3(CH_2)_2CHO$, CF_3CH_2CHO [14], and CF_3CHO [11–13]. When the number of methylene groups of the hydrocarbon chain increases, the $n \rightarrow \pi^*$ transition band exhibits a hyperchromic effect at wavelengths lower than ca. 320 nm.

$$\forall\lambda < 320\,\mathrm{nm} \quad \sigma_\lambda(CF_3(CH_2)_2CHO) > \sigma_\lambda(CF_3CH_2CHO) > \sigma_\lambda(CF_3CHO)$$

However, as a consequence of the shift of the $n \rightarrow \pi^*$ band to longer wavelengths (bathochromic effect), the former trend in σ_λ changes:

$$\forall\lambda > 320\,\mathrm{nm} \quad \sigma_\lambda(CF_3(CH_2)_2CHO) < \sigma_\lambda(CF_3CH_2CHO) < \sigma_\lambda(CF_3CHO)$$

In Table 1, $\sigma_{\lambda,max}$ for $CF_3(CH_2)_2CHO$ is compared with those for shorter hydrofluoroaldehydes. At 298 K, averaged absorption cross section of $(5.85 \pm 0.14) \times 10^{-20}$ and $(5.84 \pm 0.16) \times 10^{-20}$ cm^2 molecule^{-1} were determined for $CF_3(CH_2)_2CHO$ at (290.9 ± 0.8) nm and (283.3 ± 0.9) nm, respectively. $\sigma_{\lambda,max}$ for $CF_3(CH_2)_2CHO$ is higher than those for CF_3CHO at 301 nm and CF_3CH_2CHO at 290.8 nm [11–14].

3.2. FTIR identification and quantification of end-photolysis products

As mentioned in the previous section and similarly to CF_3CH_2CHO [14], the photolysis experiments in air were carried out in the presence of a large excess of cyclohexane (C_6H_{12}) to scavenge OH radicals. These radicals are likely to be formed in the cell from the reaction of $CF_3(CH_2)_2CO$ formed in channel (1c) with O_2, similar to CH_3CO and C_2H_5CO radicals [21–25]:

$$CF_3(CH_2)_2CO + O_2 \rightarrow OH + \text{co-products} \qquad \text{(2a)}$$

The OH formation in reaction (2a) competes with the association reaction at high total pressures:

$$CF_3(CH_2)_2CO + O_2 + M \rightarrow CF_3(CH_2)_2C(O)O_2 + M \qquad \text{(2b)}$$

From $CF_3(CH_2)_2C(O)O_2$ radicals, 4,4,4-trifluorobutanoic acid ($CF_3(CH_2)_2C(O)OH$) can be formed by reaction with HO_2 radicals (produced in the HCO + O_2 reaction):

$$CF_3(CH_2)_2C(O)O_2 + HO_2 \rightarrow CF_3(CH_2)_2C(O)OH + O_3 \qquad (3)$$

In the presence of OH-scavenger, $CF_3(CH_2)_2C(O)OH$ was not detected (it can be below the detection limit), indicating that $CF_3(CH_2)_2CO$ radicals are not significantly formed in the primary process (1c). In contrast, $CF_3(CH_2)_2C(O)OH$ (a band centered around 3580 cm^{-1}) and F_2CO (1850–2000 cm^{-1}) were identified in the absence of OH-scavenger (see spectrum in Fig. S1 of the supporting information). Gaseous $CF_3(CH_2)_2C(O)OH$ could not be quantified, since the reference spectrum was recorded by flowing He through solid $CF_3(CH_2)_2C(O)OH$. Under these conditions, the formation of $CF_3(CH_2)_2C(O)OH$ seems to be due to the formation of $CF_3(CH_2)_2CO$ radicals:

$$OH + CF_3(CH_2)_2CHO \rightarrow CF_3(CH_2)_2CO + H_2O \qquad (4)$$

An example of the FTIR spectrum of the $CF_3(CH_2)_2CHO/C_6H_{12}$/air mixtures recorded in the dark is presented in Fig. 3a. After 10 min of irradiation, CO (2034–2238 cm^{-1}), CF_3CH_2CHO (shoulder around at 1760 cm^{-1}), HC(O)OH (peak at 1776 cm^{-1}) were identified (Fig. 3b). Since the selected IR band for $CF_3(CH_2)_2CHO$ lies in the C=O stretching region, the features of other carbonyl compounds, such as CF_3CH_2CHO and HC(O)OH, might be subtracted in that spectral region in order to properly obtain the photolysis quantum yield (Eq. (E6)). Measured concentration ranges of the end-products were the following: $(3.65–28.8) \times 10^{15}$ molecule cm^{-3} for CO, $(2.18–66.8) \times 10^{14}$ molecule cm^{-3} for CF_3CH_2CHO, $(0.28–17.4) \times 10^{14}$ molecule cm^{-3} for HC(O)OH and $(0.11–15.6) \times 10^{14}$ molecule cm^{-3} for CF_3CHO. $CF_3CH_2CH_2OH$ was also observed. After subtracting a reference spectrum of these final products, the residual spectra did not show any unidentified species (an example is shown in Fig. 3b).

In the presence of added O_2, the formation of CO is consistent with the rapid conversion of HCO radicals formed in channel (1a):

$$HCO + O_2 \rightarrow HO_2 + CO \qquad (5)$$

In the absence of added O_2 (experiments with N_2), apart from reaction (1b) if formed, CO can also be produced in the thermal decomposition of $CF_3(CH_2)_2CO$ radicals formed in reaction (1c):

$$CF_3(CH_2)_2CO + M \rightarrow CF_3(CH_2)_2 + CO + M \qquad (6)$$

The amount of CO formed in the experiments performed in N_2 bath gas was similar to that observed in the presence of O_2. This was attributed to the effect of a small leak (less than 1 mTorr of air) that quickly converts HCO into CO. Therefore, under static conditions and with time scales on the order of minutes it is hard to distinguish the direct CO formation from channel (1b) and the indirect CO from reaction (6).

The formation of CF_3CH_2CHO is consistent with the secondary chemistry in the presence of O_2 initiated by HCO and $CF_3(CH_2)_2$ radicals formed in channel (1a):

$$CF_3(CH_2)_2 + O_2 + M \rightarrow CF_3(CH_2)_2O_2 + M \qquad (7)$$

$$2CF_3(CH_2)_2O_2 \rightarrow 2CF_3(CH_2)_2O + O_2 \qquad \text{(8a)}$$

$$\rightarrow CF_3CH_2CHO + CF_3CH_2CH_2OH + O_2 \qquad \text{(8b)}$$

$$CF_3(CH_2)_2O + O_2 \rightarrow CF_3CH_2CHO + HO_2 \qquad (9)$$

From the reaction sequence (7)–(9), it is clear that $CF_3CH_2CH_2OH$ can also be formed, but in a lesser extent than CF_3CH_2CHO. However, the concentration of CF_3CH_2CHO can be reduced by 308-nm photolysis, yielding CF_3CHO [14]. Like in the 308-nm photolysis of CF_3CH_2CHO, the source of HC(O)OH

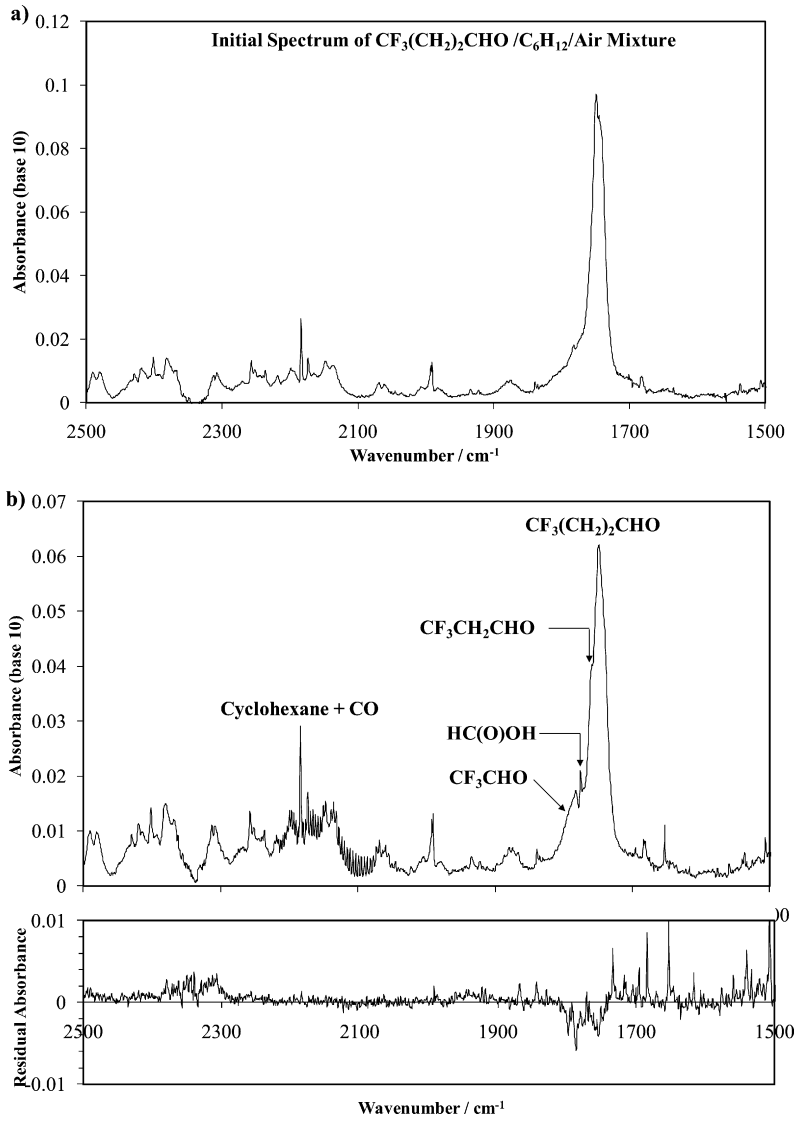

Fig. 3. FTIR spectra of the $CF_3(CH_2)_2CHO$/air mixture. (a) Before irradiation, $[CF_3(CH_2)_2CHO]_0$,$_{Photol.Cell}$ = 9.8×10^{15} molecule cm^{-3}, $[cyclohexane]_{Photol.Cell}$ = 3.3×10^{17} molecule cm^{-3} and p_T = 170 Torr. (b) After 6000 pulses of irradiation, bands for products are identified. (c) After spectral subtraction of the CF_3CH_2CHO, CF_3CHO, and HC(O)OH features.

is not clear. In our work, the [HC(O)OH]/[CO] ratio depends on the consumed fluorinated aldehyde, $\Delta[CF_3(CH_2)_2CHO]$. This ratio varies from less than 1% for $CF_3(CH_2)_2CHO$ losses of 3.2×10^{15} molecule cm^{-3} to less than 5% for $CF_3(CH_2)_2CHO$ losses of 1.8×10^{16} molecule cm^{-3}. HC(O)OH formation could be related with the secondary chemistry of formaldehyde (CH_2O) which can be formed by thermal decomposition of $CF_3(CH_2)_2O$ radicals:

$$CF_3(CH_2)_2O \rightarrow CF_3CH_2 + CH_2O \quad (10)$$

HC(O)OH can be formed via the following reaction sequence:

$$HO_2 + CH_2O \rightarrow HOCH_2OO \quad (11)$$

$$2HOCH_2OO \rightarrow HC(O)OH + CH_2(OH)_2 + O_2 \quad (12a)$$

$$\rightarrow 2HOCH_2O + O_2 \quad (12b)$$

$$HOCH_2OO + HO_2 \rightarrow HOCH_2COOH + O_2 \quad (13a)$$

$$\rightarrow HC(O)OH + H_2O + O_2 \quad (13b)$$

$$\rightarrow HOCH_2O + OH + O_2 \quad (13c)$$

Since in the presence of an excess of O_2, reactions (9) and (10) can compete, CH_2O and, therefore, HC(O)OH will be formed in a greater or a lesser extent depending on the corresponding rate coefficients. A numerical simulation on the HC(O)OH formation was performed using Facsimile program. k_9 was taken as 1.0×10^{-14} cm^3 molecule^{-1} s^{-1} corresponding to that for the $CH_3(CH_2)_2O + O_2$ reaction [20] and k_{10} was considered equal to that for the thermal decomposition of $CH_3(CH_2)_2O$ radicals, 8.0×10^4 s^{-1} [26]. The simulated concentrations of HC(O)OH were one order of magnitude lower that the experimentally observed. Moreover, under our experimental conditions, formaldehyde was not observed in the final IR spectra.

Another proposed source of HC(O)OH can be the reaction of stabilized $HC(O)O_2$ molecular complex [27,28] formed in reaction (5), which could react with HO_2 radicals (similar to $CH_3C(O)O_2$ radicals [29,30]) to form HC(O)OH. Further studies are needed to corroborate this hypothesis.

Our results are consistent with those reported by Tadić et al. [31] for the photolysis of butanal, n-C_3H_7CHO. End-products formed in the steady-state photolysis of butanal between 275 and 380 nm

Table 2
Photolysis quantum yields of $CF_3(CH_2)_2CHO$ at 308 nm as a function of total pressure of air.

p_T/Torr	[M] × 10^{-19}/molecule cm^{-3}	$\Phi_{\lambda=308nm}$
20.5	0.066	0.89 ± 0.02
29.9	0.097	0.74 ± 0.03
45.0	0.15	0.71 ± 0.03
75.3	0.24	0.58 ± 0.07
99.3	0.32	0.45 ± 0.02
170.3	0.55	0.39 ± 0.03
250.6	0.81	0.33 ± 0.05
400.6	1.29	0.27 ± 0.05
520.2	1.68	0.23 ± 0.01
550.1	1.78	0.20 ± 0.01
640.3	2.07	0.20 ± 0.01
696.0	2.26	0.19 ± 0.01
760.5	2.46	0.16 ± 0.01

were detected by FTIR spectroscopy. The products observed were CO, C_2H_4, CH_3CHO, CH_2CHOH and CO_2, indicating that the photolysis of n-C_3H_7CHO undergoes Norrish type I (ϕ_{14a}) and Norrish type II (ϕ_{14c}) dissociation [31]:

$$n\text{-}C_3H_7CHO + h\nu(\lambda = 275\text{–}380\,nm) \rightarrow n\text{-}C_3H_7 + HCO \quad (14a)$$

$$\rightarrow C_3H_8 + CO \quad (14b)$$

$$\rightarrow C_2H_4 + CH_2CHOH \quad (14c)$$

$$\rightarrow CH_3 + CH_2CH_2CHO \quad (14d)$$

$$\rightarrow C_3H_6 + HCHO \quad (14e)$$

Therefore, channels (14b, 14d, and 14e) are unimportant at wavelengths > 280 nm. Vinyl alcohol (CH_2CHOH) and acetaldehyde are in equilibrium:

$$CH_2CHOH \rightleftarrows CH_3CHO \quad (15)$$

At 1 bar of air, the branching ratio ϕ_{14a}/ϕ_{14c} is 2.1. In $CF_3(CH_2)_2CHO$, a Norrish type II reaction is not possible, since there is no γ-hydrogen atoms susceptible to be removed by intramolecular abstraction. Thus, the substitution of a -CF_3 group in butanal eliminates the competition between Norrish type I and II.

3.3. Pressure dependence of the photolysis quantum yield of $CF_3(CH_2)_2CHO$ at 308 nm

Once the spectral subtraction of CF_3CH_2CHO, CF_3CHO, and HC(O)OH is performed, the C=O stretching band of $CF_3(CH_2)_2CHO$ was used to quantify this species at a given number of laser pulses. An example of the plots of Eq. (E6) for $CF_3(CH_2)_2CHO$ and CH_3CHO is presented in Fig. 4a. Taking into account σ_λ for $CF_3(CH_2)_2CHO$ determined here at 308 nm, $(3.43 \pm 0.04) \times 10^{-20}$ cm^2 molecule^{-1}, the averaged photolysis quantum yield at different total pressures is reported in Table 2. As can be seen, $\Phi_{\lambda=308\,nm}$ decreases from 0.89 at 20 Torr to 0.16 at 760 Torr. In Fig. 4b, the Stern–Volmer (SV) plot for $\Phi_{\lambda=308\,nm}$ is shown. As can be seen, the SV plot exhibits a slight curvature at low total pressures. A curvature in the SV plots was previously observed for acetone [32,33] and for methylethylketone and diethylketone [22] at excitation wavelengths greater than 300 and 308 nm, respectively. Blitz et al. [32] interpreted the observed curvature of the SV plot as an evidence of the dissociation from two excited states of acetone, the singlet state (S_1) at λ < 300 nm and S_1 and the triplet state (T_1) at λ > 300 nm. Therefore, it seems that multiple electronic states are involved

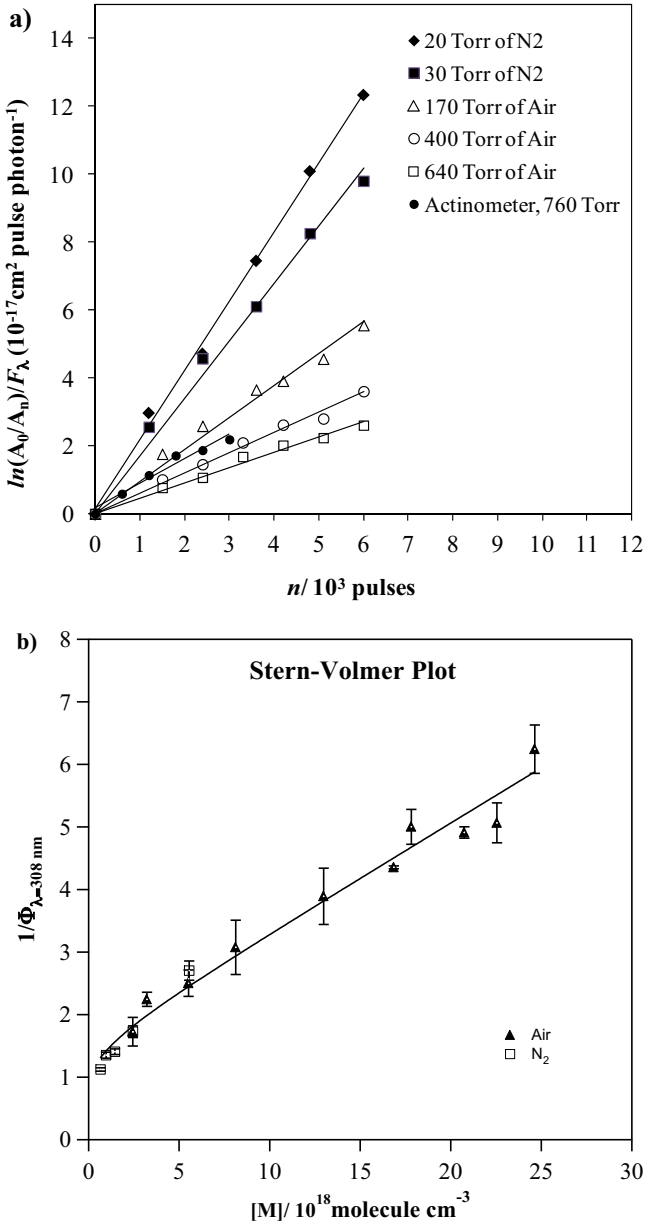

Fig. 4. (a) Decays of the integrated areas, A_n, corrected by F_λ for $CF_3(CH_2)_2CHO$ as a function of total pressure and for CH_3CHO at 760 Torr ($[\,]_{0,Photol.Cell} = 3.6 \times 10^{16}$ molecule cm^{-3}). (b) Stern–Volmer plot for the photolysis quantum yield at 308 nm for $CF_3(CH_2)_2CHO$.

in the photolysis of $CF_3(CH_2)_2CHO$ and a similar mechanism is proposed:

$$S_0 + h\nu(\lambda = 308\,nm) \rightarrow S_1$$

$S_1 + M \rightarrow S_0 + M$	k_{MS}
$S_1 \rightarrow$ Dissociation products	k_{dS}
$S_1 \rightarrow T_1$	k_{ISC}
$T_1 + M \rightarrow S_0 + M$	k_{MT}
$T_1 \rightarrow$ Dissociation products	k_{dT}

k_{MS} and k_{MT} are the quenching rate coefficients for S_1 and T_1, respectively. k_{dS} and k_{dT} are the dissociation rate coefficients for S_1 and T_1, respectively, and k_{ISC} is the intersystem crossing rate coefficient.

At low total pressures the slight curvature can be interpreted by the population of T_1 by intersystem crossing from S_1.

Dissociation from T_1 is also possible at low pressures. According to that mechanism, the SV plots can be described by the following equation [32]:

$$\frac{1}{\Phi_{\lambda=308\ \mathrm{nm}}} = \frac{(1+a_2+a_1[\mathrm{M}])(1+a_3[\mathrm{M}])}{1+a_2+a_3[\mathrm{M}]} \quad \text{(E10)}$$

where $a_1 = k_{MS}/k_{dS}$, $a_2 = k_{ISC}/k_{dS}$ and $a_3 = k_{MT}/k_{dT}$, where $\Phi^0_{\lambda=308\,\mathrm{nm}}$ is taken as unity. In the high-pressure regime, Eq. (E10) is simplified as:

$$\frac{1}{\Phi_{\lambda=308\ \mathrm{nm}}} \approx 1 + a_2 + a_1[\mathrm{M}] \quad \text{(E11)}$$

From the slope of the SV plot at high pressures, $a_1 = k_{MS}/k_{dS} = (1.71 \pm 0.17) \times 10^{-19}$ cm^3 molecule^{-1} is derived and a_2 was obtained ($k_{ISC}/k_{dS} = 0.62 \pm 0.11$) from the intercept of such a plot. Under these conditions, the photolysis mechanism occurs exclusively by the dissociation of S_1. In Fig. 4b, a fit of the data to Eq. (E10) is depicted by a solid line. a_2 was fixed in the analysis of data, getting $a_1 = (1.76 \pm 0.06) \times 10^{-19}$ cm^3 molecule^{-1} and $a_3 = (1.44 \pm 0.84) \times 10^{-18}$ cm^3 molecule^{-1}.

At tropospheric pressures, the high-pressure SV equation should be an adequate description of the photolysis of $CF_3(CH_2)_2CHO$. Under our experimental conditions, the gas mixtures approximately contain 74% of N_2, 19% of O_2, 6% of cyclohexane and 0.2% of $CF_3(CH_2)_2CHO$ at all pressures. Since [M] is the sum of the concentration of all possible quenchers present, Eq. (E11) can be rewritten as:

$$\left(\frac{\Phi^0}{\Phi}\right)_{\lambda=308\ \mathrm{nm}} = 1 + \frac{k_{O_2}}{k_{dS}}[O_2] + \frac{k_{N_2}}{k_{dS}}[N_2] + \frac{k_{CHex}}{k_{dS}}[C_6H_{12}] + \frac{k_{SQ}}{k_{dS}}[CF_3(CH_2)_2CHO] \quad \text{(E12)}$$

k_i (i = O_2, N_2, C_6H_{12}) are the quenching rate coefficient for these gases and k_{SQ}, is the rate coefficient for the self-quenching. Taking into account the composition of the gas mixture, it is simplified to:

$$\left(\frac{\Phi^0}{\Phi}\right)_{\lambda=308\ \mathrm{nm}} = 1 + \left\{\frac{0.19k_{O_2}}{k_{dS}} + \frac{0.74k_{N_2}}{k_{dS}} + \frac{0.06k_{CHex}}{k_{dS}} + \frac{0.002k_{SQ}}{k_{dS}}\right\}[\mathrm{M}] \quad \text{(E13)}$$

At high pressures, cyclohexane and $CF_3(CH_2)_2CHO$ concentrations are sufficiently low to affect the quenching of S_1, even if an upper limit of 10^{-10} cm^3 molecule^{-1} s^{-1} is considered for the corresponding quenching rate coefficients. In all cases the main contributor to collisional deactivation of S_1 is the bath gas.

Indirect quantum yield measurements of butanal were reported by Tadić et al. between 275 and 380 nm [31]. The pressure quenching of butanal was reported to be weaker than that observed for $CF_3(CH_2)_2CHO$. The obtained photolysis quantum yield for butanal at zero pressure was 0.55 and the Stern–Volmer constant was 5.96×10^{-20} cm^3 molecule^{-1} [31]. These authors also attributed the deviation of unity of Φ^0_λ to the existence of other energy-dissipating processes, possibly, the deactivation of the triplet state of butanal by phosphorescence.

4. Conclusions

In conclusion, we present the first photochemical study of 4,4,4-trifluorobutanal, $CF_3(CH_2)_2CHO$. Absorption cross sections, $\sigma_\lambda(T)$, were determined as a function of wavelength (230–340 nm) and temperature (269–323 K). Additionally, the photolysis quantum yields of $CF_3(CH_2)_2CHO$ at 308 nm, $\Phi_{\lambda=308\,\mathrm{nm}}$, are reported here between 20.5 and 760 Torr. A negative pressure dependence of $\Phi_{\lambda=308\,\mathrm{nm}}$ was observed, i.e. $\Phi_{\lambda=308\,\mathrm{nm}}$ decreases at high total pressures. A slight curvature in the Stern–Volmer plot was noticeable at low pressures, indicating that two excited states of $CF_3(CH_2)_2CHO$ (the singlet S_1 and triplet T_1 states) seem to be involved in the dissociation mechanism. For atmospheric modeling purposes, the derived high-pressure SV equation should be an adequate description of the photolysis of $CF_3(CH_2)_2CHO$.

In the presence of air, the photolysis of $CF_3(CH_2)_2CHO$ at 308 nm mainly produces HCO and $CF_3(CH_2)_2$ radicals, which in the presence of O_2 finally form CO, HC(O)OH, CF_3CH_2CHO, and $CF_3CH_2CH_2OH$. Further photodegradation of CF_3CH_2CHO yields shorter fluoroaldehydes and fluoroalcohols.

Acknowledgements

The authors would like to thank the Spanish Ministerio de Ciencia e Innovación (MICINN) (CGL2007-61835/CLI and CGL2010-19066) and the Consejería de Educación y Ciencia de la Junta de Comunidades de Castilla-La Mancha (PAI-05-062 and PEII11-0279-8538) for supporting this Project. Also, M. Antiñolo wishes to thank MICINN for providing her a grant.

Appendix A. Supplementary data

Supplementary data associated with this article can be found, in the online version, at doi:10.1016/j.jphotochem.2011.12.023.

References

[1] http://www.epa.gov.
[2] X. Tang, S. Madronich, T. Wallington, D. Calamari, Changes in tropospheric composition and air quality, J. Photochem. Photobiol. B 46 (1998) 83–95.
[3] Ch. George, J.Y. Saison, J.L. Ponche, Ph. Mirabel, Kinetics of mass transfer of carbonyl fluoride, trifluoroacetyl fluoride, and trifluoroacetyl chloride at the air/water interface, J. Phys. Chem. 98 (1994) 10857–10862.
[4] M.D. Hurley, T.J. Wallington, M.P. Sulbaek Andersen, D.A. Ellis, J.W. Martin, S.A. Mabury, Atmospheric chemistry of fluorinated alcohols: reaction with cl atoms and oh radicals and atmospheric lifetimes, J. Phys. Chem. A 108 (2004) 1973–1979.
[5] S.R. Sellevåg, C.J. Nielsen, O.A. Søvde, G. Myhre, J.K. Sundet, F.I. Stordal, S.A. Isaken, Atmospheric gas-phase degradation and global warming potentials of 2-fluoroethanol, 2,2-difluoroethanol, and 2,2,2-trifluoroethanol, Atmos. Environ. 38 (2004) 6725–6735.
[6] M.D. Hurley, J.C. Misner, J.A. Ball, T.J. Wallington, D.A. Ellis, S.A. Mabury, Atmospheric chemistry of $CF_3CH_2CH_2OH$: kinetics, mechanisms and products of Cl atom and OH radical initiated oxidation in the presence and absence of NO_x, J. Phys. Chem. A 109 (2005) 9816–9826.
[7] T. Kelly, V. Bossoutrot, I. Magneron, K. Wirtz, J. Treacy, A. Mellouki, H. Sidebottom, G. Le Bras, A kinetic and mechanistic study of the reactions of OH radicals and Cl atoms with 3,3,3-trifluoropropanol under atmospheric conditions, J. Phys. Chem. A 109 (2005) 347–355.
[8] D.J. Scollard, J.J. Treacy, H.W. Sidebottom, C. Balestra-Garcia, G. Laverdet, G. Lebras, H. MacLeod, S. Teton, Rate constants for the reactions of hydroxyl radicals and chlorine atoms with halogenated aldehydes, J. Phys. Chem. 97 (1993) 4683–4688.
[9] M.P. Sulbaek Andersen, O.J. Nielsen, M.D. Hurley, J.C. Ball, T.J. Wallington, J.E. Stevens, J.W. Martin, D.A. Ellis, S.A. Mabury, Atmospheric chemistry of n–$C_xF_{2x+1}CHO$ (x = 1, 3, 4): reaction with Cl atoms, OH radicals and IR spectra of $C_xF_{2x+1}C(O)O_2NO_2$, J. Phys. Chem. A 108 (2004) 5189–5196.
[10] M. Antiñolo, E. Jiménez, A. Notario, E. Martínez, J. Albaladejo, Tropospheric photooxidation of CF_3CH_2CHO and $CF_3(CH_2)_2CHO$ initiated by Cl atoms and OH radicals, Atmos. Chem. Phys. 10 (2010) 1911–1922.
[11] S.R. Sellevåg, T. Kelly, H. Sidebottom, C.J. Nielsen, A study of the IR and UV–vis absorption cross-sections, photolysis and OH-initiated oxidation of CF_3CHO and CF_3CH_2CHO, Phys. Chem. Chem. Phys. 6 (2004) 1243–1252.
[12] Y. Hashikawa, M. Kawasaki, R.L. Waterland, M.D. Hurley, J.C. Ball, T.J. Wallington, M.P. Sulbaek Andersen, O.J. Nielsen, Gas phase UV and IR absorption spectra of $C_xF_{2x+1}CHO$ (x = 1–4), J. Fluoresc. Chem. 125 (2004) 1925–1932.
[13] M.S. Chiappero, F.E. Malanca, G.A. Argüello, S.T. Wooldridge, M.D. Hurley, J.C. Ball, T.J. Wallington, R.L. Waterland, R.C. Buck, Atmospheric chemistry of perfluoroaldehydes ($C_xF_{2x+1}CHO$) and fluorotelomer aldehydes ($C_xF_{2x+1}CH_2CHO$): quantification of the important role of photolysis, J. Phys. Chem. A 110 (2006) 11944–11953.
[14] M. Antiñolo, E. Jiménez, J. Albaladejo, UV absorption cross sections between 230 and 350 nm and pressure dependence of the photolysis quantum yield at 308 nm of CF_3CH_2CHO, Phys. Chem. Chem. Phys. 13 (2011) 15936–15946.

[15] E. Jiménez, B. Lanza, E. Martínez, J. Albaladejo, Daytime tropospheric loss of hexanal and *trans*-2-hexenal: OH kinetics and UV photolysis, Atmos. Chem. Phys. 7 (2007) 1565–1574.
[16] B. Lanza, E. Jiménez, B. Ballesteros, J. Albaladejo, Absorption cross section determination of biogenic C_5-aldehydes in the actinic region, Chem. Phys. Lett. 454 (2008) 184–189.
[17] E. Jiménez, B. Lanza, M. Antiñolo, J. Albaladejo, Photooxidation of leaf-wound oxygenated compounds, 1-penten-3-ol, (*Z*)-3-hexen-1-ol, and 1-penten-3-one, initiated by OH radicals and sunlight, Environ. Sci. Technol. 43 (2009) 1831–1837.
[18] E. Jiménez, M. Antiñolo, B. Ballesteros, E. Martinez, J. Albaladejo, Atmospheric lifetimes and global warming potentials of $CF_3CH_2CH_2OH$ and $CF_3(CH_2)_2CH_2OH$, Chem. Phys. Chem. 11 (2010) 4079–4087.
[19] G.K. Moortgart, H. Meyrahn, P. Warneck, Photolysis of acetaldehyde in air: CH_4 CO and CO_2 quantum yields, Chem. Phys. Chem. 11 (2010) 3896–3908.
[20] R. Atkinson, D.L. Baulch, R.A. Cox, J.N. Crowley, R.F. Hampson, R.G. Hynes, M.E. Jenkin, M.J. Rossi, J. Troe, Evaluated kinetic and photochemical data for atmospheric chemistry: volume II – gas phase reactions of organic species, Atmos. Chem. Phys. 6 (2006) 3625–4055.
[21] M.A. Blitz, D.E. Heard, M.J. Pilling, OH formation from $CH_3CO + O_2$: a convenient experimental marker for the acetyl radical, Chem. Phys. Lett. 365 (2002) 374–379.
[22] M.T. Baeza Romero, M.A. Blitz, D.E. Heard, M.J. Pilling, B. Price, P.W. Seakins, L. Wang, Photolysis of methylethyl, diethyl and methylvinyl ketones and their role in the atmospheric budget, Faraday Discuss. 130 (2005) 73–88.
[23] S.A. Carr, M.T. Baeza-Romero, M.A. Blitz, M.J. Pilling, D.E. Heard, P.W. Seakins, OH yields from the $CH_3CO + O_2$ reaction using an internal standard, Chem. Phys. Lett. 445 (2007) 108–112.
[24] S.A. Carr, D.R. Glowacki, C. Liang, M.T. Baeza-Romero, M.A. Blitz, M.J. Pilling, P.W. Seakins, Experimental and modeling studies of the pressure and temperature dependences of the kinetics and the OH yields in the acetyl + O_2 reaction, J. Phys. Chem. A 115 (2011) 1069–1085.
[25] M.T. Baeza Romero, M.A. Blitz, D.E. Heard, M.J. Pilling, B. Price, P.W. Seakins, OH formation from $C_2H_5CO + O_2$ reaction: an experimental marker for the propionyl radical, Chem. Phys. Lett. 445 (2005) 232–236.
[26] H. Curran, Rate constant estimation for C_1 to C_4 alkyl and alkoxyl radical decomposition, Int. J. Chem. Kinet. 38 (2006) 250–275.
[27] A.O. Langford, C.B. Moore, Collision complex formation in the reactions of formyl radicals with nitric oxide and oxygen, J. Chem. Phys. 80 (1984) 4211–4221.
[28] J.W. Bozelli, A.M. Dean, Hydrocarbon radical reactions with O_2: comparison of allyl, formyl, and vinyl to ethyl, J. Phys. Chem. 97 (1993) 4427–4441.
[29] T.J. Dillon, J.N. Crowley, Direct detection of OH formation in the reactions of HO_2 with $CH_3C(O)O_2$ and other substituted peroxy radicals, Atmos. Chem. Phys. 8 (2008) 4877–4889.
[30] M.E. Jenkin, M.D. Hurley, T.J. Wallington, Investigation of the radical product channel of the $CH_3(CO)O_2 + HO_2$ reaction in the gas phase, Phys. Chem. Chem. Phys. 9 (2007) 3149–3162.
[31] J. Tadić, I. Juranic, G.K. Moortgat, Pressure dependence of the photooxidation of selected carbonyl compounds in air: *n*-butanal and *n*-pentanal, J. Photochem. Photobiol. A: Chem. 143 (2001) 169–179.
[32] M.A. Blitz, D.E. Heard, M.J. Pilling, Study of acetone photodissociation over the wavelength range 248–330 nm: evidence of a mechanism involving both the singlet and triplet excited states, J. Phys. Chem. A 110 (2006) 6742–6756.
[33] R. Nadasdi, G. Kovács, I. Szilágyi, A. Demeter, S. Dóbé, T. Bercés, F. Márta, Exciplez laser photolysis of acetone with relevance to tropospheric chemistry, Chem. Phys. Lett. 440 (2007) 31–35.